ChemComm

COMMUNICATION

View Article Online
View Journal | View Issue

Cite this: *Chem. Commun.*, 2025, 61, 9884

Received 23rd April 2025,
Accepted 21st May 2025

DOI: 10.1039/d5cc01463h

rsc.li/chemcomm

Insight into the effects of pulsed CO_2 electrolysis in a zero-gap electrolyzer†

Xiao Kun Lu, [a] Weiyan Ni,[bc] Adrien E. Deberghes[a] and Linsey C. Seitz *[a]

Electrochemical CO_2 reduction reactions face activity, selectivity, and stability challenges as this technology moves towards commercialization. Pulsed electrolysis (PE) has been shown to improve selectivity and stability at the cost of a negligible energy increase. The effectiveness of PE was assessed in a zero-gap membrane electrode assembly with a Cu catalyst between 50 and 500 mA cm^{-2} with various, widely adopted binders including Nafion, Sustainion, and fluorinated ethylene propylene. PE suppresses H_2 production at 50–300 mA cm^{-2} and nearly doubles the faradaic efficiency of multi-carbon products when this approach is combined with the use of Sustainion-incorporating electrodes. We find that the notable improvement can be accounted for *via* the increased local CO_2 concentration observed using *in situ* surface enhanced Raman spectroscopy.

Of the myriad electrochemical CO_2 reduction (ECR) products, selectivity for multi-carbon products (C_{2+}) remains below the selectivity requirements (>80% faradaic efficiency (FE)[1]) due to complex reaction pathways and high activation barriers.[2–4] Catalyst tuning has attracted much of the recent research attention to alter the binding strength of *CO,[5,6] while fewer studies have focused on operational approaches to increase C_{2+} selectivity.

Improving FE through identification of an optimal potential/current density window is a simple technique ubiquitously performed in static electrolysis. Pulsed electrolysis (PE) is a technique where the cathode applied potential/current density is changed between two values (E_a or j_a and E_c or j_c, a = anodic and c = cathodic values) within time intervals, t_a and t_c.[7] PE studies have focused on optimizing the E_a and time periods for various purposes. PE has been shown to increase selectivity towards the desired products through local reaction environment modification when E_a results in a j_a close to no current.[8–10] PE also modulates catalyst faceting when E_a is more anodic than the Cu oxidation redox potentials.[11,12] Finally, PE prolongs the stability of both the catalyst[13–15] and the gas diffusion layer (GDL)[16] through regenerative processes when E_a stops the ECR. However, the majority of the previous FE enhancement results were obtained in H-type cells and flow cells. As commercialization of ECR calls for >3000 h of stability,[17,18] the effect of PE in zero-gap membrane electrode assembly (MEA) devices needs to be assessed.

In this study, we explored the effects of binding agents on PE in an MEA. We further characterize the local reaction environment using a GDL-based *in situ* Raman cell that better represents the GDE geometry compared to commonly used H-type Raman cells. Finally, we examined the stability of anodes under PE and evaluated the stability number for catalyst precious metal dissolution.

Three types of binders were assessed for enhancement under PE in zero-gap MEA devices: (1) Nafion, a cation exchange binder that contains a fluorinated backbone and a sulfonic acid functional group,[19] (2) Sustainion, an anion exchange binder with an imidazolium functional group,[20] and (3) fluorinated ethylene propylene (FEP) for hydrophobic treatment (Fig. S1, ESI†).[21] Binders were chosen to vary the local H_2O and CO_2 transport, which greatly influences the response to PE.[8]

Gas diffusion electrodes (GDEs) were prepared by spray coating a sonicated ink of 50 nm Cu NPs, isopropanol, and binder onto a carbon paper GDL with a microporous layer (Fig. S2–S5, ESI†). The GDEs with FEP, Nafion, and Sustainion have decreasing hydrophobicity based on water contact angle measurements, showing 132°, 128°, and 124°, respectively (Fig. S6, ESI†).

ECR performance was evaluated in an anion exchange MEA device with a 0.1 M $KHCO_3$ anolyte and an IrO_x/Ti anode prepared by a dip-coating method (Fig. S7–S9, ESI†).[22] Current densities of 50–500 mA cm^{-2} were applied *via* GS chronopotentiometric (CP) holds, or PE CPs, switching between j_a = 1 and j_c = 50–500 mA cm^{-2} at t_a = 20 s "off" and t_c = 40 s "on" intervals (Fig. S10, ESI†). A non-zero j_a prevents returning to open circuit potential (OCP), which may cause Ti transport layer

[a] *Department of Chemical and Biological Engineering, Northwestern University, Evanston, IL 60208, USA. E-mail: linsey.seitz@northwestern.edu*
[b] *Department of Chemistry, Northwestern University, Evanston, IL 60208, USA*
[c] *Department of Electrical and Computer Engineering, Northwestern University, Evanston, IL 60208, USA*

† Electronic supplementary information (ESI) available. See DOI: https://doi.org/10.1039/d5cc01463h

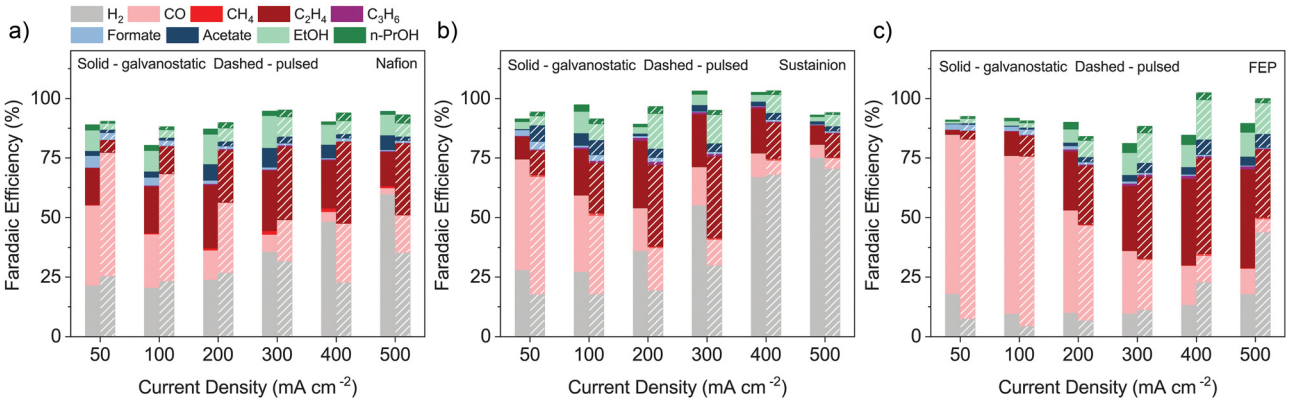

Fig. 1 FEs of H_2, C_1, and C_{2+} products for electrodes comprising Cu NPs and (a) Nafion, (b) Sustainion, or (c) FEP binders under GS and PE operation.

degradation.[23] Studies have utilized various t_a values for local reaction environment modulation ($t_a > 0.6$ s) or catalyst regeneration ($t_a > 5$ min).[15,16] We chose a t_a of 20 s in agreement with a previous report that shows mitigation of salt precipitates using PE and a t_c of 40 s to match the timescales of our characterization techniques.[16]

Fig. 1 and Fig. S11 (ESI†) show the FE of GDEs fabricated with the three binders under GS and PE operations. Under GS operation, the FEP-GDE at <200 mA cm^{-2} shows hydrogen evolution reaction (HER) suppression, at just 10% FE towards H_2. However, the main product at <200 mA cm^{-2} is CO. Ionomer-based GDEs, the Nafion-GDE and the Sustainion-GDE, achieved higher C_{2+} product production at <200 mA cm^{-2}. Ion conducting groups may enable C_{2+} production at lower current densities.

For GS operation between 200 and 500 mA cm^{-2}, the C_{2+} FE of the FEP-GDE increases from 36% to 60%, while the Nafion-GDE and Sustainion-GDE exhibit C_{2+} FEs that continuously decrease as the current density increases. The Sustainion-GDE only shows an 18% FE towards ECR products at 500 mA cm^{-2}. The ability to maintain C_{2+} production at a high current density can be ascribed to the hydrophobicity of the binder. Low hydrophobicity may cause flooding of the GDE and hinder CO_2 transport.[24,25] This is exacerbated by the applied potential due to electrowetting.[26,27]

The FEP-GDE in PE exhibits an increased CO FE at <200 mA cm^{-2}, while the Nafion-GDE exhibits an increased CO FE at all current densities, compared to GS operation. The CO FE is less impacted by PE *vs.* GS operation for the Sustainion-GDE. For PE between 50 and 300 mA cm^{-2}, the C_{2+} FE of the Nafion-GDE is lower compared to that for GS operation, while the H_2 FE is lower between 300 and 500 mA cm^{-2}. Similarly, the FEP-GDE has a higher CO FE at 50 and 100 mA cm^{-2} with good HER suppression. The Sustainion-GDE under PE also exhibits good HER suppression (Fig. 1d–f); at 200 mA cm^{-2}, the HER only comprises 20% FE, while C_{2+} products comprise 56% FE. This is explained by the increased concentration of local CO_2 due to PE, and the ability of Sustainion to stabilize ECR intermediates for further reduction. The Sustainion-GDE under PE still suffers from flooding, and the HER is the predominant reaction at >400 mA cm^{-2}.

The Sustainion-GDE exhibiting a high C_{2+} FE at a lower operating current density could reduce the operating cost since the peak energy efficiency and economic benefits of ECR plummet at high current densities according to technoeconomic analysis.[28] Anionic species (*e.g.*, OH^- and HCO_3^-) transported across the anion exchange membranes have lower ionic conductivity compared to H^+ in proton exchange membranes; hence, operating anion exchange MEAs at high currents induces higher ohmic overpotential. ECR devices also drive inefficient water oxidation due to the near-neutral electrolytes.[29] The improved C_{2+} FE at 200 mA cm^{-2} for the Sustainion-GDE could be of great interest as it balances faradaic and energy efficiencies.

PE enhancement effects originate from the changes in the local reaction environment, which are further corroborated by the use of ionomer binders. Nafion as a cation exchange ionomer may trap the OH^- produced by the ECR or HER in the vicinity of the catalyst particles, yielding a higher local pH to suppress the HER.[8,30] Sustainion allows for higher dissolution of CO_2 at the catalyst interface, and its imidazolium functional group has also been shown to stabilize $*CO_2^-$, which further utilizes the high local CO_2 concentration for CO_2 conversion.[8,31]

In situ surface enhanced Raman spectroscopy (SERS) was performed in a GDE-based spectro-electrochemical cell to understand the origin of the PE enhancement with the use of a Sustainion binder (Fig. S12, ESI†). CuO was chosen as a catalyst for Raman study to ensure a focused beam onto the electrode surface at OCP (the start of the experiment) so that changes in signal intensity at various potentials are not a result of change in focal length. CuO is reduced to Cu under ECR conditions. Fig. S16 and Table S1 (ESI†) show the full SERS spectra and peak assignments of CuO/Sustainion-GDEs under GS and PE operation ranging from OCP to -1.6 V_{RHE}. The operating potentials are chosen so that Raman spectra could reflect $*CO_3^{2-}$ adsorption rather than *CO adsorption.

The two main findings from *in situ* SERS experiments are that the local CO_2 concentration and local pH are increased during PE compared to GS operation. Fig. 2a shows that the Cu–$*CO_2^-$ peak intensity (at 362 cm^{-1}) increases as the applied potential is stepped cathodically, from -1.0 to -1.6 V_{RHE} under GS operations.[32,33] The Cu–$*CO_2^-$ peak intensity under PE is higher than that of their GS operated counterparts at -1.0 and -1.3 V_{RHE}

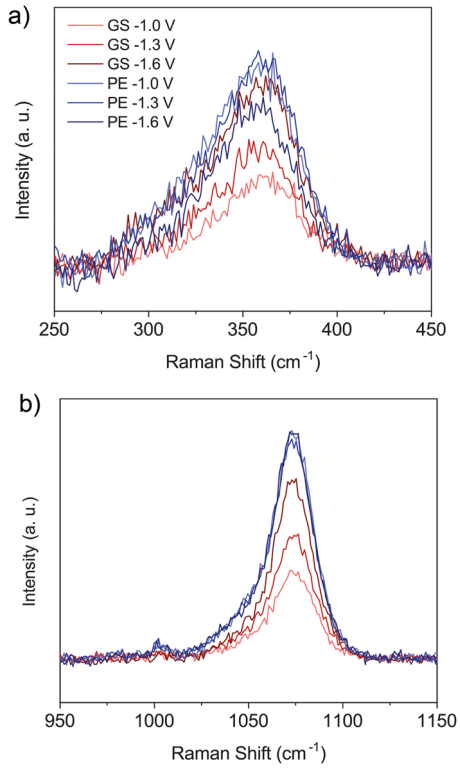

Fig. 2 *In situ* SERS spectra for (a) Cu–$*CO_2^-$ stretching and (b) $*CO_3^{2-}$ peaks during GS, CP and PE of the CuO/Sustainion-GDE in a GDE-based Raman cell with 0.1 M $KHCO_3$.

with the maximum intensity at −1.3 V *vs.* RHE for PE rather than at −1.6 V_{RHE} for GS operation. Local CO_2 regeneration during the "off" time of PE is the reason for the higher $*CO_2^-$, which leads to enhanced ECR performance and HER suppression.

Fig. 2b shows the $*CO_3^{2-}$ peak intensity (at 1073 cm^{-1}). Previous studies have used HCO_3^-/CO_3^- peak ratios to calculate the local pH, but in the present system, CO_3^{2-} is the only dominant species and would not lead to accurate values of local pH.[34] The $*CO_3^{2-}$ peak intensity during GS operation increases as the potential becomes more negative due to the production of OH^- as a side ECR or HER product. The $*CO_3^{2-}$ peak intensities during the "on" periods of all three PE conditions were higher than those of their GS counterparts. This may arise from the higher local CO_2 concentration due to PE. Switching of electrical potential during PE allows for accumulation of the produced OH^- and CO_2-neutralized CO_3^{2-} rather than repulsion from the cathode.[10]

It is noteworthy that Ir-based anode catalysts contribute to a significant amount of capital expenditure of CO_2 electrolyzers. Due to the (bi)carbonate equilibrium, even when alkaline electrolytes are used, the anodic local pH is neutral-acidic and can cause dissolution of 3d-transition metal-based catalysts (*e.g.*, Ni), making Ir indispensable in CO_2 MEA electrolyzers for their stability under acidic OER conditions.[35,36] PE may benefit ECR from multiple perspectives as described previously, but the stability of Ir-based anodes under PE remains unclear.

The stability of the IrO_x/Ti anode under PE was examined over ~5700 cycles (1 min per cycle totaling to ~4 days of continuous testing) between j_c = 200 mA cm^{-2} and j_a = 1 mA cm^{-2}. The HER was chosen as the cathodic reaction since the overpotential and degradation rate are hypothesized to be much lower than those for the OER or ECR; therefore, the changes in potential response for this system primarily reflect the stability of the anode. The local pH of the anode when operating in neutral buffer is predicted to be ~3 due to consumption of OH^-.[29]

Fig. 3a shows the potential response of the water electrolyzer under PE. We took average full cell potentials (over 10 cycles) at 0 cycles, 500 cycles, and each time before and after the electrolyte was replaced (Fig. S20–S22, ESI†). The full cell potentials increased after each electrolyte replacement, from ~3.10 V to ~3.36 V, with the exception of the initial electrolyte replacement after 30 minutes of conditioning (Fig. 3b). The number of cycles that the system requires to reach stabilized operation also increases with the number of times the electrolyte is replaced. Changes in full cell potential are attributed to the pH change at the cathode after electrolyte replacement. The catholyte reaches a pH of 12–13 after 1400 cycles due to the lack of CO_2 in the system to buffer the cathodic pH. In an actual CO_2 MEA, electrolyte replacement would not have drastic impacts on the cathodic half-cell potential. The anolyte pH remains at ~7, yielding a similar OER environment to an actual CO_2 electrolyzer. In contrast, the steady operation full cell potential does not increase starting from the ~900th cycle to the ~5660th cycle, suggesting that the anode catalyst does not undergo significant degradation due to pulsing over the timescale that we examined.

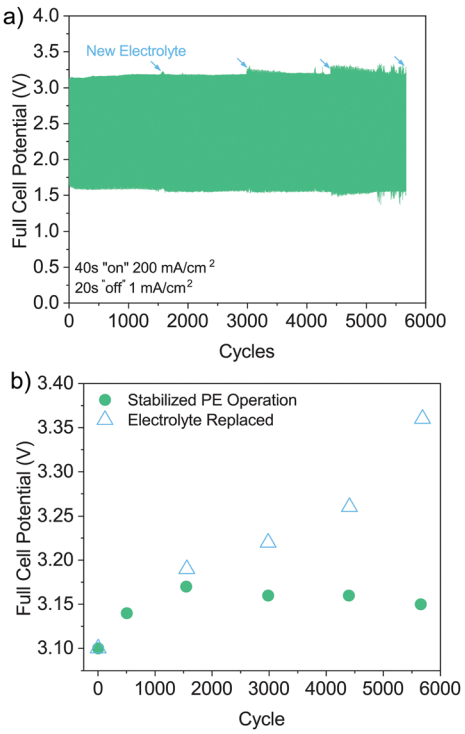

Fig. 3 (a) Potential response of near-neutral water electrolysis under PE at 200 mA cm^{-2} with the Pt/C cathode and the IrO_x/Ti anode in the 0.1 M $KHCO_3$ anolyte. (b) Average full cell potential (over 10 cycles) before ("steady state" under PE) and after electrolyte replacement periods.

The stability number (S-number) is defined as the ratio of the O_2 molecules produced to Ir atoms dissolved. The S-number of the IrO_x/Ti anode under PE post-testing is 5×10^5, determined by inductively coupled plasma mass spectrometry of Ir in the anolyte and the digested AEM. The S-numbers of the aqueous media system and MEA are 10^4–10^5 and 10^6–10^9, respectively.[37,38] In a CO_2 electrolyzer, the IrO_x anode forms interfaces with both a liquid electrolyte and an AEM, which yields a unique system with a combination of MEA and aqueous media.

In summary, ECR in a zero-gap MEA can be enhanced by PE between 50 and 300 mA cm^{-2}, which is likely due to the increased CO_2 concentration and local pH, as verified by *in situ* SERS. With the Sustainion binder, a 56% FE for C_{2+} species was achieved using commercial Cu NP under PE, almost double that of its GS counterpart. HER suppression and enhancement to CO formation were also observed for electrodes with FEP or Nafion binders. The Ir anode stability of near-neutral water oxidation in MEA in PE can be predicted *via* the S-number, which falls in between the aqueous media and MEA due to the presence of the 0.1 M $KHCO_3$ anolyte. PE provides a promising pathway to enhance the ECR with just ~1% of energy consumption; however, the dilution of the product stream due to down time requires technoeconomic assessment to identify the optimal balance of stability and performance.[16,39]

Data availability

The data supporting this article have been included as part of the ESI.†

Conflicts of interest

There are no conflicts to declare.

References

1 E. W. Lees, B. A. W. Mowbray, F. G. L. Parlane and C. P. Berlinguette, *Nat. Rev. Mater.*, 2022, **7**, 55–64.
2 A. J. Garza, A. T. Bell and M. Head-Gordon, *ACS Catal.*, 2018, **8**, 1490–1499.
3 J. H. Montoya, A. A. Peterson and J. K. Nørskov, *ChemCatChem*, 2013, **5**, 737–742.
4 T.-C. Kuo, J.-W. Chou, M.-H. Shen, Z.-S. Hong, T.-H. Chao, Q. Lu and M.-J. Cheng, *J. Phys. Chem. C*, 2021, **125**, 2464–2476.
5 S. Nitopi, E. Bertheussen, S. B. Scott, X. Liu, A. K. Engstfeld, S. Horch, B. Seger, I. E. L. Stephens, K. Chan, C. Hahn, J. K. Norskov, T. F. Jaramillo and I. Chorkendorff, *Chem. Rev.*, 2019, **119**(12), 7610–7672, DOI: 10.1021/acs.chemrev.8b00705.
6 S. Du, P. Yang, M. Li, L. Tao, S. Wang and Z. Liu, *Chem. Commun.*, 2024, **60**, 1207–1221.
7 R. Casebolt, K. Levine, J. Suntivich and T. Hanrath, *Joule*, 2021, **5**, 1987–2026.
8 C. Kim, J. C. Bui, X. Luo, J. K. Cooper, A. Kusoglu, A. Z. Weber and A. T. Bell, *Nat. Energy*, 2021, **6**, 1026–1034.
9 C. Kim, L.-C. Weng and A. T. Bell, *ACS Catal.*, 2020, **10**, 12403–12413.
10 A. Herzog, M. Lopez Luna, H. S. Jeon, C. Rettenmaier, P. Grosse, A. Bergmann and B. Roldan Cuenya, *Nat. Commun.*, 2024, **15**, 3986.
11 J. Timoshenko, A. Bergmann, C. Rettenmaier, A. Herzog, R. M. Arán-Ais, H. S. Jeon, F. T. Haase, U. Hejral, P. Grosse, S. Kühl, E. M. Davis, J. Tian, O. Magnussen and B. Roldan Cuenya, *Nat. Catal.*, 2022, **5**, 259–267.
12 H. S. Jeon, J. Timoshenko, C. Rettenmaier, A. Herzog, A. Yoon, S. W. Chee, S. Oener, U. Hejral, F. T. Haase and B. Roldan Cuenya, *J. Am. Chem. Soc.*, 2021, **143**, 7578–7587.
13 Y. Jännsch, J. J. Leung, M. Hämmerle, E. Magori, K. Wiesner-Fleischer, E. Simon, M. Fleischer and R. Moos, *Electrochem. Commun.*, 2020, **121**, 106861.
14 T. N. Nguyen, Z. Chen, A. S. Zeraati, H. S. Shiran, S. M. Sadaf, M. G. Kibria, E. H. Sargent and C. T. Dinh, *J. Am. Chem. Soc.*, 2022, **144**, 13254–13265.
15 J. Kok, J. de Ruiter, W. van der Stam and T. Burdyny, *J. Am. Chem. Soc.*, 2024, **146**, 19509–19520.
16 Y. Xu, J. P. Edwards, S. Liu, R. K. Miao, J. E. Huang, C. M. Gabardo, C. P. O'Brien, J. Li, E. H. Sargent and D. Sinton, *ACS Energy Lett.*, 2021, **6**, 809–815.
17 E. W. Lees, B. A. W. Mowbray, F. G. L. Parlane and C. P. Berlinguette, *Nat. Rev. Mater.*, 2021, **7**, 55–64.
18 C. P. O'Brien, D. McLaughlin, T. Böhm, Y. C. Xiao, J. P. Edwards, C. M. Gabardo, M. Bierling, J. Wicks, A. Sedighian Rasouli, J. Abed, D. Young, C.-T. Dinh, E. H. Sargent, S. Thiele and D. Sinton, *Joule*, 2024, **8**, 2903–2919.
19 P. Ding, H. An, P. Zellner, T. Guan, J. Gao, P. Müller-Buschbaum, B. M. Weckhuysen, W. van der Stam and I. D. Sharp, *ACS Catal.*, 2023, **13**, 5336–5347.
20 Z. Liu, H. Yang, R. Kutz and R. I. Masel, *J. Electrochem. Soc.*, 2018, **165**, J3371.
21 T. H. M. Pham, J. Zhang, M. Li, T. H. Shen, Y. Ko, V. Tileli, W. Luo and A. Züttel, *Adv. Energy Mater.*, 2022, **12**, 2103663.
22 W. Luc, J. Rosen and F. Jiao, *Catal. Today*, 2017, **288**, 79–84.
23 A. Weiß, A. Siebel, M. Bernt, T. H. Shen, V. Tileli and H. A. Gasteiger, *J. Electrochem. Soc.*, 2019, **166**, F487.
24 Y. Wu, L. Charlesworth, I. Maglaya, M. N. Idros, M. Li, T. Burdyny, G. Wang and T. E. Rufford, *ACS Energy Lett.*, 2022, **7**, 2884–2892.
25 Z. Xing, L. Hu, D. S. Ripatti, X. Hu and X. Feng, *Nat. Commun.*, 2021, **12**, 136.
26 K. Yang, R. Kas, W. A. Smith and T. Burdyny, *ACS Energy Lett.*, 2020, **6**, 33–40.
27 M. Li, M. N. Idros, Y. Wu, T. Burdyny, S. Garg, X. S. Zhao, G. Wang and T. E. Rufford, *J. Mater. Chem. A*, 2021, **9**, 19369–19409.
28 S. C. da Cunha and J. Resasco, *Nat. Commun.*, 2023, **14**, 5513.
29 C. P. O'Brien, R. K. Miao, A. Shayesteh Zeraati, G. Lee, E. H. Sargent and D. Sinton, *Chem. Rev.*, 2024, **124**(7), 3648–3693, DOI: 10.1021/acs.chemrev.3c00206.
30 M. Li, E. W. Lees, W. Ju, S. Subramanian, K. Yang, J. C. Bui, H.-P. Iglesias van Montfort, M. Abdinejad, J. Middelkoop, P. Strasser, A. Z. Weber, A. T. Bell and T. Burdyny, *Nat. Commun.*, 2024, **15**, 8222.
31 B. A. Rosen, A. Salehi-Khojin, M. R. Thorson, W. Zhu, D. T. Whipple, P. J. A. Kenis and R. I. Masel, *Science*, 2011, **334**, 643–644.
32 Y. Zhao, X.-G. Zhang, B. Nataraju, W. Yang, Q. Liang, P. Radjenovic, Y.-H. Wang, Y.-J. Zhang, J.-C. Dong, Z.-Q. Tian and J.-F. Li, *Energy Environ. Sci.*, 2022, **15**, 3968–3977, DOI: 10.1039/d2ee01334g.
33 I. V. Chernyshova, P. Somasundaran and S. Ponnurangam, *Proc. Natl. Acad. Sci. U. S. A.*, 2018, **115**, E9261–E9270.
34 D. A. Henckel, M. J. Counihan, H. E. Holmes, X. Chen, U. O. Nwabara, S. Verma, J. Rodríguez-López, P. J. A. Kenis and A. A. Gewirth, *ACS Catal.*, 2020, **11**, 255–263.
35 Á. Vass, B. Endrődi, G. F. Samu, Á. Balog, A. Kormányos, S. Cherevko and C. Janáky, *ACS Energy Lett.*, 2021, **6**, 3801–3808.
36 Á. Vass, A. Kormányos, Z. Kószó, B. Endrődi and C. Janáky, *ACS Catal.*, 2022, **12**, 1037–1051.
37 J. Knöppel, M. Möckl, D. Escalera-López, K. Stojanovski, M. Bierling, T. Böhm, S. Thiele, M. Rzepka and S. Cherevko, *Nat. Commun.*, 2021, **12**, 2231.
38 J. Edgington and L. C. Seitz, *ACS Catal.*, 2023, **13**, 3379–3394.
39 Y. L. Chung, S. Kim, Y. Lee, D. T. Wijaya, C. W. Lee, K. Jin and J. Na, *iScience*, 2024, **27**, 110383.